HHS Public Access

Author manuscript

Nat Immunol. Author manuscript; available in PMC 2018 January 24.

Published in final edited form as:

Nat Immunol. 2017 September ; 18(9): 1025–1034. doi:10.1038/ni.3808.

Metabolic control of the scaffold protein TKS5 in tissue-invasive, pro-inflammatory T cells

Yi Shen[1], **Zhenke Wen**[1], **Yinyin Li**[1], **Eric L. Matteson**[2], **Jason Hong**[1], **Jörg J. Goronzy**[1], and **Cornelia M. Weyand**[1,†]

[1]Division of Immunology and Rheumatology, Department of Medicine, Stanford University School of Medicine, Stanford, CA 94305, USA

[2]Division of Rheumatology, Mayo Clinic College of Medicine, Rochester, MN 55905, USA

Abstract

Pathogenic T cells in rheumatoid arthritis (RA) infiltrate non-lymphoid tissue sites, maneuver through extra-cellular matrix and form lasting inflammatory microstructures. Here, we found that RA T cells abundantly express the podosome scaffolding protein TKS5, enabling them to form tissue-invasive membrane structures. TKS5 overexpression was regulated by the intracellular metabolic environment of RA T cells; specifically, reduced glycolytic flux resulting in ATP and pyruvate deficiencies. ATP^{lo}, $pyruvate^{lo}$ conditions triggered fatty acid biosynthesis and the formation of cytoplasmic lipid droplets. Restoring pyruvate production or inhibiting fatty acid synthesis corrected the tissue-invasiveness of RA T cells *in vivo* and reversed their pro-arthritogenic behavior. Thus, metabolic control of T cell locomotion provides new opportunities to interfere with T cell invasion into specific tissue sites.

The autoimmune syndrome rheumatoid arthritis (RA) causes relentless joint inflammation, eventually damaging cartilage and bone[1]. T cells are key pathogenic drivers sustaining synoviocyte proliferation, tissue inflammation, neoangiogenesis, bony erosion and autoantibody formation[2,3]. RA T cells age at a faster rate, acquiring aged phenotypes 20 years prematurely[4,5]. Functionally, they are prone to differentiate into proinflammatory effector cells, producing excess inflammatory cytokines and amplifying the inflammatory activity of non-T cells in the synovial tissue[6,7].

The bias of RA T cells to commit to proinflammatory effectors functions is mechanistically linked to defective metabolic regulation[8–10]. Specifically, they fail to sufficiently upregulate the glycolytic enzyme PFKFB3, curbing lactate and ATP generation[11]. Instead, they shunt glucose into the pentose-phosphate pathway (PPP), hyperproduce NADPH, and accumulate

†Correspondence should be addressed to C.M.W. (cweyand@stanford.edu).

Data availability

All data that support the findings of this study are available from the corresponding author upon request at cweyand@stanford.edu.

Author contributions: CMW, YS and JJG designed the study and analyzed the data. YS, ZW and YL performed experiments. YS created all of the figures. EM and JH were responsible for patient selection, evaluation and recruitment. CMW, YS and JJG wrote the manuscript.

reduced glutathione[8,9,11] causing insufficient activation of the redox-sensing kinase ATM, a cell-cycle regulator and DNA repair molecule[9,12]. ROS^{lo} ATM^{lo} RA T cells bypass the G2/M cell-cycle checkpoint, hyperproliferate and accelerate naive-to-memory conversion. ATM deficiency deviates RA T cells towards T_H1 and T_H17 differentiation, a phenotype corrected by replenishing ROS[9].

The PPP enables cells to build chemical constituents for macromolecule synthesis, such as DNA, RNA, proteins and membranes[13]; a critical prerequisite for biomass generation during massive T cell expansion[14]. The PPP product NADPH functions as a reducing agent for anabolic reactions, such as lipid and cholesterol biosynthesis[15–17]. Glucose delivers carbon for various lipid classes, but most of the *de novo* synthesized fatty acids (FA) are incorporated into phospholipids for membrane biogenesis[18,19] and localize to lipid rafts to participate in crucial membrane-based processes[20]. The rate-limiting step of FA biosynthesis generates malonyl-CoA from acetyl-CoA by acetyl-CoA carboxylase 1 (*ACACA*)[21]. Subsequent synthetic steps and FA elongation require fatty acid synthase (*FASN*), stearoyl-CoA desaturase (*SCD*), and the fatty acid-coenzyme A ligase family to generate diacetylglycerols, triacetylglycerols and long-chained FA[16]. Through mitochondrial β-oxidation, FA catabolism feeds NADH and $FADH_2$ into the electron transport chain and generates acetyl-CoA to fuel the citric acid cycle[17,22]. T cells depend on glucose, amino acids and lipids as energy sources, but their metabolic preferences are tightly linked to particular life cycle stages[17,23,24].

Pathogenic T cell functions in RA include the trafficking to the joint, diapedesis into the matrix, transit within the tissue and building of compact microarchitectures[25]. T cell diapedesis from the vessels involves formation of “invasive podosomes” to build transcellular pores[26]. Once in the matrix, T cells resort to nonproteolytic migration, maneuvering through extracellular space with an amoeba-like movement, adaptively changing shape to crawl along collagen fibrils and squeezing through preexisting matrix gaps[27]. Such T cell mobility requires dynamic formation of cell protrusions, regulated by the cellular cytoskeleton to accomplish cellular spreading, polarization and ultimately cell motion. Small Rho family GTPases activate actin filament assembly factors to form sheet-like lamellopodia and ruffles and finger-like filopodia and microvilli[28,29]. The adaptor molecule TKS5 is critically involved in determining localization of membrane protrusions[30]. TKS5 clustering at the plasma membrane facilitates F-actin assembly and enhances the interaction of multiple proteins assembled in podosomes, including the nucleation promoting factor, N-WASP[30], the SH3/SH2 adaptor, Grb2[30], ADAM-family metalloproteases, and the adhesion receptor, dystroglycan[31].

RA T cells serve as an excellent model system to define the molecular underpinning of pathogenic T cell behavior. Previous studies have defined a state of metabolic reprogramming in RA T cells: as $PFKFB3^{lo}$, $G6PD^{hi}$ cells, they divert glucose away from energy production towards biosynthetic fitness[8,9,11]. Here, we show that the rewiring of cellular metabolism renders RA T cells tissue invasive, directly promoting disease-inducing effector functions. The ATP^{lo}, $pyruvate^{lo}$, $NADPH^{hi}$ metabolic state induced an energy storage mode with excess synthesis of FA and cytoplasmic lipid droplet (LD) deposition. This resulted in an upregulated T cell locomotion program, high production of the podosome

scaffolding protein TKS5 and ultimately a functional phenotype of hypermotility. TKS5^{hi} RA T cells spontaneously formed actin- and cortactin-rich membrane ruffles, empowering them to penetrate into non-lymphoid tissue and establish lasting inflammatory infiltrates. Two metabolic interferences corrected the tissue invasiveness of RA T cells; enhancing activity of pyruvate kinase or disrupting the downstream effect of excessive lipid storage by targeting FA synthase. Both interventions amended TKS5 overproduction, prevented T cell entry into synovial tissue and provided effective protection from tissue inflammation *in vivo*.

RESULTS

RA T cells upregulate the locomotion program

A key pathogenic property of RA T cells is their ability to rapidly invade the synovial membrane, maneuver through extravascular space and polarize into pro-inflammatory effector cells[11,32]. Tissue infrastructure and chemokine milieu contribute to the attraction and retention of T cells[32,33]. We explored whether RA T cells have intrinsic defects that enhance their tissue invasiveness.

To understand the T cell locomotion program, we first probed the migratory capacity of RA and healthy human activated naïve CD4$^+$ T cells in a chemokine-free system. Almost double as many RA CD4$^+$ T cells as healthy control cells migrated through porous membranes, even in the absence of a chemotactic gradient (Fig. 1a). To determine potential factors influencing CD4$^+$ T cell motility, we examined their amoeba-like motion through extracellular matrix in a 3D-collagen gel system, also a chemokine-free system. Stimulated CD4$^+$ T cells were loaded onto the gel surface, matrix-infiltrating cells marked with the nuclear stain DAPI and invasion depth quantified by optical sectioning every 100 μm (Fig. 1b–d). Compared to healthy cells, more RA CD4$^+$ T cells entered the collagenous matrix and moved further within the matrix [distance of 700 compared to 500 μm (Fig. 1b–d)].

Following an early period of random walk, T cells form organized membrane extension for directed motion[32]. We thus analyzed cell shape and membrane protrusions in proliferating RA and control CD4$^+$ T cells (Fig. 1e–f). Considering cortactin's involvement in lamellipodia and invadopodia formation[29,34], we quantified expression of this core element of the locomotion program. Protein expression of cortactin and the cytoskeletal protein F-actin were more than doubled in patient-derived cells (Fig. 1f). Healthy CD4$^+$ T cells displayed a thin peripheral actin cortex, whereas F-actin and cortactin clustered in broad-based membrane ruffles in RA cells (Fig. 1e). Merged F-actin-cortactin expression was seven-fold higher in patient-derived cells (Fig. 1f).

We subsequently compared healthy and RA CD4$^+$ T cells for the expression of a core group of genes associated with the cell's locomotion machinery. T cells were stimulated, gene expression was analyzed by RT-PCR after 72 h. In a cohort of 6 patient-control pairs, 10 motility-related genes had consistently higher expression in patient-derived T cells (Fig. 1g). Specifically, RA T cells expressed higher transcript levels of *SH3PXD2A* (which encodes the TKS5 protein)[35], an adaptor molecule facilitating the formation and stabilization of cellular projections. Flow cytometry confirmed overexpression of TKS5 (Fig. 1h–i).

To examine the pathogenic relevance of aberrant TKS5 expression in patient-derived T cells, we investigated the propensity of tissue invasion in a chimeric mouse model. Human synovium was implanted into NSG mice and human T cells were adoptively transferred into the chimeras[9,33,36]. Synovium-invasive T cells were tracked by immunohistochemistry as well as gene expression profiling in the explanted tissue grafts (Fig. 1j–l). Few healthy T cells infiltrated the synovial tissue (Fig. 1j–l). Transfer of RA PBMC produced a dense T cell infiltrate. Knockdown of *SH3PXD2A* (Supplementary Fig. 1) prior to adoptive transfer disrupted the invasive capabilities of RA T cells (Fig. 1m–o). Conversely, TKS5 overexpression (Supplementary Fig. 1) in healthy T cells resulted in enhanced T cell invasion, such that $TKS5^{hi}$ control T cells mimicked patient-derived T cells (Fig. 1p–r). We then tested whether TKS5 expression in activated $CD4^+CD45RA^+$ T cells collected from RA patients correlated with the clinical activity of their joint disease. Patients with higher disease activity measured through clinical disease activity indices (CDAI) transcribed progressively higher levels of *SH3PXD2A* mRNA in their T cells (Fig. 1s; R = 0.63).

Thus, RA T cells were equipped to dynamically form membrane ruffles, spread, and move and with a spontaneous upregulation of their locomotion gene module rapidly invaded into non-lymphoid tissue sites. The scaffolding protein TKS5 appeared to be non-redundant for this invasive behavior.

TKS5 expression is metabolically regulated

A key characteristic of RA T cells is their metabolic reprogramming. Specifically, RA T cells shunt glucose away from glycolysis towards the PPP, producing less ATP but more NADPH than healthy counterparts[9,11,17]. We therefore explored whether the T cell locomotion module is under metabolic control. We mimicked the slowed glycolytic breakdown in RA T cells by treating healthy $CD4^+$ T cells with the PFKFB3 inhibitor, 3PO (200 nM, 72 h). Conversely, we treated patient-derived T cells with the FAS inhibitor C75 (20 μM, 72 h) to inhibit increased NADPH-dependent fatty acid synthesis. Concentrations of the inhibitors were chosen based on dose-response experiments (Supplementary Fig. 2). Expression of the TKS5-encoding gene *SH3PXD2A* was highly sensitive to metabolic interference. PFKFB3 blockade increased while FAS inhibition diminished *SH3PXD2A* transcript levels (Fig. 2a–b). Five additional genes from the locomotion module normalized in C75-treated RA T cells. PFKFB3 inhibition effectively enhanced motility gene expression by >50% for 8 of the 10 genes tested (Fig. 2c). Flow cytometric analysis was used to assess TKS5 protein expression. PFKFB3 inhibition increasedTKS5 mimicking the phenotype of RA T cells (Fig. 2d–e, h–j). Vice versa, reduced FA synthesis corrected the TKS5 overexpression in RA T cells, restoring a normal phenotype (Fig. 2f–g, k–m). These data directly implicated glycolytic activity and FA synthesis as regulatory steps in locomotion function, broadening the impact of metabolic control on normal and pathogenic T cell effector functions.

Aberrant lipid biosynthesis in RA T cells

To further characterize the lipid biosynthesis program of RA T cells, possibly altered due to the increased generation of NADPH in the PPP, we activated naive $CD4^+CD45RA^+$ T cells from RA patients and age-matched controls by TCR crosslinking for 96 h and quantified

cytoplasmic lipid stores. Patients with psoriatic arthritis (PsA) served as disease controls. Bodipy staining demonstrated accumulation of cytoplasmic neutral lipids in RA T cells, with Bodipy intensity 8-fold higher in RA T cells compared to control and PsA T cells (Fig. 3a–b). Naive as well as memory CD4 T cells from RA patients accumulated cytoplasmic lipid droplets (LD) (Fig. 3c). To test whether LD formation occurs in RA patients *in vivo*, we stained tissue sections from RA synovial biopsies. Synovial T cells resembled *ex vivo* stimulated T cells, harboring densely packed lipid bodies in their cytoplasm (Fig. 3d). As an additional read-out of lipid biosynthesis, we quantified palmitic acid (C-16) in stimulated T cells from healthy individuals, RA patients and PsA patients. Significantly elevated palmitic acid concentrations were a distinguishing characteristic of RA T cells (Fig. 3e). Finally, we analyzed the gene module relevant for the process of droplet formation, including *BSCL2*, *PLIN1*, and *FSP27*. Expression for all three genes was selectively higher in RA T cells compared to healthy and PsA T cells (Fig. 3f). Thus, RA T cells, including tissue inflammatory T cells, were committed to an anabolic lipid-biosynthesis program, leading to cytoplasmic storage of excess FA. The shift towards anabolic metabolism occurred in the setting of reduced glycolytic activity and overall energy starvation.

To better understand the process of LD accumulation, we analyzed gene expression of key lipid biosynthesis molecules in a discovery cohort of 10 RA patients and age-matched controls. Purified $CD4^+CD45RA^+$ T cells were stimulated with anti-CD3/CD28-coated beads for 72 h. RT-PCR analysis demonstrated markedly higher expression of 20 lipogenesis genes in patient-derived T cells (Fig. 4a), which was confirmed in a validation cohort of 6 patients and 6 matched controls (Fig. 4b). Most significant changes were seen in enzymes facilitating *de novo* FA synthesis (*ACACA, FASN, SCD*) and esterification (*ACSL3, 4, 5, 6* and *DGAT1, 2*). Three of five genes relevant for mitochondrial β-oxidation (*HADHA, HADHB, ACADM*) were expressed at significantly higher levels in RA T cells.

Kinetic studies showed no differences of *ACACA, FASN* and *SCD* transcripts in resting cells but higher induction in RA T cells 2–6 days after activation (Fig. 4c). Immunoblotting confirmed markedly higher expression of the corresponding proteins (Fig. 4d).

Not all genes related to intracellular lipid homeostasis were affected by the shunting towards lipid anabolism in RA T cells. Carnitine palmitoyltransferase I (CPT1) regulates the carnitine-dependent cytoplasm-to-mitochondria transport of long-chain fatty acyl-CoAs. *CPT1A* and *B* expression were indistinguishable in control and RA T cells (Fig. 4e). Also, genes involved in cholesterol biosynthesis, previously reported as critical in early expansion of $CD8^+$ effector T cells[37], were not part of the metabolic signature distinguishing RA T cells from healthy controls (Fig. 4f). The lipid storage in RA T cell was highly sensitive to inhibition of FAS with 20 μM C75, which cleared cytoplasmic LDs (Fig. 4g–j) placing this enzyme at the pinnacle of altered lipid biosynthesis program.

In summary, upon activation, RA T cells induced a broad, yet selective, lipogenic gene program focused on FA and LD formation, but sparing cholesterol production.

Relationship of lipid droplet formation to glycolytic activity

Next, we aimed to connect the processes of glycolysis, lipid droplet formation and T cell locomotion. Quantification of core metabolites at the interface of glycolysis and FA synthesis demonstrated that RA T cells were low in pyruvate and ATP amounts, but had elevated levels of acetyl-CoA (Fig. 5a). To mimic these conditions and generate a ATP^{lo} $pyruvate^{lo}$ state, we slowed glycolytic flux in healthy $CD4^+$ T cells by treatment with the PFKFB3 inhibitor 3PO (200 nM) or the PK inhibitor Shikonin (250 nM) (Fig. 5b–e and Supplementary Fig. 2 and Supplementary Fig. 3). This metabolic intervention promptly induced LD formation in healthy T cells (Fig. 5b–e), mimicking the RA phenotype. We also activated lipid-synthesizing RA T cells in the presence of ML265 (10 μM), which forces PK into a highly active tetrameric formation[38,39] or treated the RA T cells with supplemental pyruvate (1 μM) (Supplementary Fig. 3). Replenishing pyruvate from extra-cellular or intra-cellular sources significantly reduced the LD load (Fig. 5f–i). Enhancing glycolytic flux through ML265 or exogenous pyruvate reduced transcript concentrations for *FASN*, a key enzyme in fatty acid synthesis (Fig. 5j), mechanistically connecting pyruvate availability with the lipogenic machinery. We considered whether the bias towards lipogenesis in RA T cells was related to activators of peroxisome proliferator-activated receptor (PPAR) signaling, although treatment of human T cells with well-established PPAR-α or PPAR-γ activators has been reported to induce a potent anti-inflammatory program, with effective suppression of pro-inflammatory cytokines[40]. PPAR-γ protein expression was similar in control and lipid-droplet-containing RA T cells and expression levels were independent of enhanced or reduced glycolytic flux (Supplementary Fig. 4), making it unlikely that PPAR-γ signaling was involved in shifting the metabolic homeostasis of RA T cells.

These results delineated a direct effect of glycolysis on lipid anabolism and indicated that pyruvate and ATP deficiency promoted *de novo* FA synthesis and cytoplasmic deposition.

PFKFB3 silencing induces tissue invasiveness

To test that the pinnacle defect in T cell hypermotility lies in insufficient glycolytic breakdown, we determined whether pharmacologic and genetic PFKFB3 impairment is able to impose the RA phenotype onto healthy T cells. Synovium-engrafted NSG mice were assigned to one of four treatment arms: reconstitution with healthy $CD4^+$ T cells transfected with control or *PFKFB3*-specific siRNA or treated with and without 3PO (200 nM). Synovitis intensity was quantified by enumerating synovial $CD3^+$ T cells and by gene expression analysis of 10 key inflammatory mediators. PFKFB3 knockdown reduced *PFKFB3*-specifc transcripts by 50% (Supplementary Fig. 5), mimicking RA T cells[9,11]. Reduction of *PFKFB3* transcript was durable over >96 h (Supplementary Fig. 5), allowing *in vivo* testing of functional consequences. Suppressing PFKFB3 function promoted aggressive T cell infiltration followed by a strong innate and adaptive inflammation (Fig. 6a–l), including expression of *TNFSF11* suggesting the recruitment and retention of $RANKL^+$ T cells and tissue production of TNF, IL-6, and IL-1β (Fig. 6f). Quantification of IFN-γ–producing effector T cells in the tissue lesions (Fig. 6d–e; Fig. 6j–k) revealed that reduced PFKFB3 function resulted in a 2–3–fold increase of synovial T cells frequencies producing this effector cytokine.

Together, these data indicated a critical role for pyruvate generation in controlling T cells' bioenergetics, tissue invasiveness and pro-inflammatory potential.

Metabolic interference corrects T cell tissue invasiveness

To investigate whether the locomotion program of RA T cells is amendable to metabolic interference *in vivo*, we employed the human synovium-NSG model system. NSG mice engrafted with human synovial tissue were reconstituted with patient-derived T cells[9,33,36]. RA T cells were highly tissue-invasive, resulting in robust synovitis with tissue expression of *TNFSF11* encoding RANKL, TNF, IL-6 and IL-1β (Fig. 7a–g). Tissue-residing T cells were characterized by expression of RANKL and strong IFN-γ and IL-17 upregulation (Fig. 7c, d, f, g) and the dominance of the lineage-determining transcription factors T-bet and RORγt (Fig. 7e). Retarding lipogenesis by inhibiting FA synthesis with C75 (5 mg/kg/mouse) efficiently suppressed tissue inflammation (Fig. 7a–g), reduced the infiltration of $RANKL^+$ T cells (Fig. 7a, b), diminished the overall density of the T cell infiltrate (Fig. 7c), and resulted in the depletion of IFN-γ^+ T cells (Fig. 7f–g). Foxp3 expression, a marker of anti-inflammatory T_{reg} cells, was unaffected (Fig. 7e). Chimeras tolerated C75 treatment with no obvious toxic effects on transferred human cells (Supplementary Fig. 6). We then restored pyruvate synthesis with the PK activator ML265 (10 mg/kg/mouse), an intervention able to correct the metabolic dysbalance in RA T cells (Fig. 5). Increased pyruvate availability resulted in striking beneficial effects *in vivo* (Fig. 7a–g). PK activation attenuated T cell accumulation, reduced TNFα and RANKL production and minimized T cell cytokines (IFN-γ, IL-17). In contrast to blocking FA synthesis, ML265 treatment left IL-6 and IL-1β gene expression unaffected (Fig. 7e). ML265 was also less potent than C75 to prevent IFN-γ^+ T cell infiltration but still highly effective (Fig. 7f–g).

These experiments demonstrated reversibility of the abnormal T cell locomotion behavior and placed defective glycolysis upstream of the tissue invasiveness of patient-derived T cells.

DISCUSSION

T cell pathogenicity depends on several functional domains, including trafficking to peripheral tissues and maneuvering in the tissue environment. Here, we define glycolytic flux and fatty acid biosynthesis as critical checkpoints in the inflammatory propensity of T cells, ultimately determining membrane configuration and tissue-invasiveness. T cells from RA patients reshape their membranes, are hypermotile and tissue-penetrating, enabling their proinflammatory effector properties in the joint. The energy-consuming process of tissue-invasion in RA T cells is linked to an ATP^{lo} $pyruvate^{lo}$ state and replenishing pyruvate is sufficient to abrogate cellular motility, tissue infiltration and inflammatory potential. The pinnacle defect appears to lie in malfunctioning glycolytic flux and shunting of glucose to the PPP, diverting energy use to a synthetic pattern. Accordingly, impairing glycolytic breakdown in healthy T cells suffices to convert them into tissue-invasive and arthritogenic effectors. Shifting the balance between catabolic and anabolic glucose utilization may provide an effective strategy to set the threshold for T cell-dependent tissue inflammation.

To minimize T cell population heterogeneity, we focused on naïve $CD4^+CD45RA^+$ T cells, which exemplify massive biomass generation demands after activation combined with needs for invasive capabilities to reach relevant tissue sites. RA T cells are distinguished from healthy counterparts by dampened glycolytic breakdown, reduced pyruvate production, and accelerated PPP shunting[8,9,11]. Instead of adopting a primarily catabolic program, they prefer anabolic biosynthesis. FA overproduction leads to cytoplasmic lipid droplet deposition commensurate with biosynthetic prerequisites for massive growth, cell-cycle passage[23] and accelerated naive-to-memory T cell conversion[17,24,41]. The price is the exhaustion of the naive T cell compartment and the accumulation of end-differentiated effector memory cells. After bypassing the G2/M cell-cycle checkpoint, RA T cells more rapidly commit to IFN-γ and IL-17 production, aborting development of anti-inflammatory T_{reg} cells[9].

Excess NADPH predicts sufficient reductive elements to drive anabolic reactions, specifically lipid-anabolic pathways. Unexpectedly, the bias towards lipid biosynthesis was selective for saponifiable lipids, while genetic modules supporting cholesterol biosynthesis remained unaffected. Newly activated $CD8^+$ T cells rapidly upregulate lipid biosynthetic pathways, synthesizing both cholesterol and FAs[37]. Sterol regulatory element-binding proteins (SREBP) control the cholesterol content in such $CD8^+$ T cells[37], acting within hours of T cell activation and impacting T cell blasting. Interestingly, homeostatic T cell proliferation and T cell pool maintenance seems SREBP-independent[37]. We propose that cellular cholesterol signals mainly during very early T cell activation, whereas later stages of T cell expansion depends on FAs.

Tissue penetration is an absolute requirement for joint-invading T cells. Beyond chemokine-guided trafficking, T cells must form membrane protrusive structures (lamellopodia, ruffles, filopodia) to maneuver through the matrix[42], while remaining proteinase-independent[27]. Membrane protrusions and amoeba-like crawling ultimately require cytoskeletal support. RA T cells are highly migratory[9] and low LSP1 expression promotes tissue and lymph node migration, exacerbating disease severity[43]. Overall, motility relies on actin nucleation in the membrane, such that an actin mesh can propel the cell across a substrate. Accordingly, we examined a core module of motility genes, covering key pathways in actin polymerization, cytoskeletal rearrangement and membrane reshaping. Higher expression of the motility gene module corresponded to hypermotility and tissue-invasiveness. Crawling through extracellular space is a membrane-centered process, hence coupling of high mobility with anabolic metabolism. Cellular ATP content appears to be of less relevance, as the highly motile T cells from RA patients are ATP^{lo}. Curbing the cells' FA content promptly downregulated many of the motility genes. Additional studies will identify the signaling cascades connecting lipid-biosynthesis with dynamic cytoskeletal and membrane shaping.

Proliferating naive T cells are glycolysis-dependent, whereas effector cells align with distinct metabolic classes[8,44]. T_{reg} cells emerge under energy-deprived conditions, with low ATP activating AMP-activated protein kinase (AMPK), curtailing mTOR and inhibiting the downstream acetyl-CoA carboxylase. Hence, low lipid biosynthesis favors T_{reg} cell differentiation[45]. This paradigm fails in RA T cells, which are pyruvate and ATP deprived[9,11], yet switch to an anabolic program. Supplementing pyruvate or enhancing

glycolytic flux efficiently cleared cytoplasmic lipid deposits and corrected the hypermigratory and hyperinflammatory phenotype of RA T cells. Thus, excess lipid storage occurred in the setting of ATP deficiency. Mitochondrial function remained intact in RA T cells and they generate sufficient citrate to support FA synthesis. However, the AMPK-controlled loop of coordinating cellular metabolism with functional behavior appears defective. Here, chronic stimulation and microenvironmental abnormalities may alter the cells' threshold settings and response patterns to metabolic cues. Experiments lowering PFKFB3 function in healthy T cells demonstrated that glycolytic slowdown is a pinnacle defect in RA T cells. Genetic or pharmacologic PFKFB3 inhibition converted healthy into arthritogenic T cells.

Current data assign metabolic checkpoint function to intracellular ATP, pyruvate and FAs in controlling disease-relevant properties. By favoring anabolic G6PD over catabolic PFKFB3, RA T cells are primed for cellular growth and differentiation. Excess FAs convey fitness for immune surveillance functions, for example leaving secondary lymphoid tissues and invading into peripheral tissues to establish long-lasting, highly efficient tertiary lymphoid structures[46]. The combination of biosynthetic precursor plus NADPH ensures active membrane biogenesis, and with sufficient ATP for survival, advances proliferation-prone and tissue-invasive T cells. Such T cells share multiple features with cancer cells, in which PPP shunting meets anabolic demands, rapid division, bypassing cell-cycle checkpoints and invadopodia formation to seed peripheral tissues with metastases[13]. AMPK regulates invadopodia formation in cancer lines, reemphasizing the mechanistic link between metabolic homeostasis and tissue invasion[47]. Lessons learned from current data should extend therapeutic strategies aimed at weakening the spread of proinflammatory T cells in RA and of malignant cells in cancer patients. Surplus FAs facilitate tissue-invasiveness and chronic inflammation in RA. The metabolic constellation of low ATP, low pyruvate and high FA could be exploited when designing highly efficient, tissue-penetrating anti-tumor T cells. Conversely, dampening the PPP, strengthening glycolytic flux, and blocking FA biosynthesis should all restrict the intrusion of T cells into susceptible tissue sites and may provide a therapeutic option for many of the chronic inflammatory conditions.

Online Methods

Patients and Controls

Demographic and clinical characteristics of 162 RA patients and 20 patients with psoriatic arthritis (PsA) enrolled at Stanford University Clinics, Stanford Hospital and the Mayo Clinic, Rochester, Minnesota are presented in Supplementary Table 1. All patients fulfilled the diagnostic criteria for RA and were positive for rheumatoid factor and/or anti-CCP antibodies. Disease activity was quantified through the Clinical Disease Activity Index (CDAI), a composite score of inflammatory load in RA patients. Individuals with cancer, uncontrolled medical disease or any other inflammatory syndrome were excluded. Healthy individuals, recruited through the Healthy Aging Cohort or the Stanford Blood Center did not have a personal or family history of autoimmune disease. The Stanford University Institutional Review Board approved the study and written informed consent was obtained

from all participants. Numbers of independent experiments or individual patients and control donors are defined in each figure legend.

T-cell preparation and culture

$CD4^+CD45RO^-$ T cells were purified by negative selection using the EasySep™ Human Naïve $CD4^+$ T Cell Enrichment Kit (STEMCELL Technologies). $CD45RO^+$ cells were targeted for removal with anti-CD45RO antibody and labeled cells were separated using an EasySep™ magnet. Subset purity monitored by FACS routinely exceeded 95% (Supplementary Fig. 7). $CD4^+CD45RO^-$ T cells (2.0×10^5/well) were stimulated with CD3/CD28-coated beads (Life Technologies AS, Oslo, Norway, ratio 1:1) and subsequently cultured for 72h or 96h, as indicated. To inhibit FA synthesis or glycolytic breakdown, cells were kept in C75 (20 μM, #10005270, Cayman Chemical) or 3PO (200 nM, #525330-25MG, EMD Millipore).

Transwell migration assay

$CD4^+CD45RA^+$ T cells were isolated and stimulated with CD3/CD28-coated beads for 24 h. 1×10^5 cells per well were cultured in cell culture inserts (#PI8P01250, Millicell) with 400 μl RPMI-1640 medium (#11875135, ThermoFisher Scientific) placed in 12-well plates that contains 600 μl RPMI-1640 medium. After 48 h, cells in the inserts or the bottom wells were collected and counted and migration rates were calculated.

3D collagen invasion assay

$CD4^+CD45RA^+$ T cells were stimulated with CD3/CD28-coated beads for 24 h. 5×10^4 cells were seeded on top of a 3D-collagen matrix (1.5 mg/ml PureCol® Bovine Collagen type I, #5005-100ML, Advanced Biomatrix), approximately 5 mm thickness). Invasion depths were measured after 48 h culture (37°C, 5% CO_2). The collagen matrix was fixed in 4% paraformaldehyde and stained with DAPI (1:1000, #D21490, ThermoFisher Scientific) for 1 h at room temperature. Individual wells filled with the collagen matrix were imaged with a LSM710 microscope using an EC Plan-Neofluar 10×/0.3 DICI objective lens (Carl Zeiss). Z-stacks were set to begin on the surface of the 3D collagen matrix and reach to the bottom of each well. Five random spots per each well were measured and the difference between the z-position of non-invading, surface-positioned cells and the deepest invading cells in the data set were recorded. Optical sections were prepared by beginning at 0 μm and cutting progressively at 100 μm intervals. The DAPI signal of each image was quantified after import into ImageJ software. The relative ratios of invading/surface cells were calculated for each measurement.

Analysis of membrane protrusive structures

5×10^4 $CD4^+CD45RA^+$ T cells were placed into 96-well plates (Corning) coated with fibronectin (10 μg/ml, # 3420-001-01, Trevigen). After 30 min at 37°C, non-adherent cells were removed and adherent cells were fixed, permeabilized and stained with anti-cortactin antibody (#PA5-29799, ThermoFisher) and rhodamine phalloidin (#R415, ThermoFisher Scientific). Nuclei were visualized with DAPI. The LSM710 system (Carl Zeiss), Plan Apochromat 63x/1.40 Oil DICIII objective lens (Carl Zeiss) was used to acquire images.

Podosome-like structures and membrane ruffles were quantified using F-actin-cortactin co-localization.

Immunohistochemical staining

Cryosections (5 μm) of explanted synovial tissues were stained with H&E and examined for the density and arrangement of inflammatory infiltrates. Synovial T cells were identified by immunohistochemical staining with mouse or rabbit Anti-Human CD3 (1:50) alone or co-stained with RANKL/CD254 (1:100) or IFN-γ (1:100) as described[9,36,48]. Sections were analyzed with an Olympus BX41 microscope, and CellSense software.

Lipid-staining fluorochromes and analysis

$CD4^+CD45RO^-$ T cells were stimulated and cultured for 96 h under standard condition before staining with BODIPY™ 493/503 (4,4-Difluoro-1,3,5,7,8-Pentamethyl-4-Bora-3a,4a-Diaza-s-Indacene) (#D3922, ThermoFisher Scientific). Cells suspensions were incubated with 3 μM BODIPY for 1 h at 37 °C, washed with 1×PBS twice, and fixed with paraformaldehyde solution, 4% in PBS (19943 1 LT, Affymetrix) for 15 min at RT. Cells were cytospun onto slides and mounted using ProLong Diamond Antifade Mountant with DAPI (P36962, ThermoFisher Scientific). Sections were imaged with a LSM710 system (Carl Zeiss); an EC Plan-Neofluar 40x/1.30 Oil DICIII objective lens (Carl Zeiss) and a Plan Apochromat 63x/1.40 Oil DICIII objective lens (Carl Zeiss) were used to acquire images. The Bodipy intensity was quantified using the LSM710 co-localization function.

Fatty acid quantification

The free fatty acid palmitic acid was measured within $CD4^+CD45RO^-$ T cells after 96 h of activation using the Free Fatty Acid Quantification Colorimetric/Fluorometric kits (K612-100, BioVision).

Pyruvate measurements

$CD4^+CD45RO^-$ T cells were stimulated with anti-CD3/CD28 beads for 72 h and pyruvate levels were quantified with Pyruvate assay kits (MAK071-1KT, Sigma-Aldrich).

Acetyl-CoA quantification

Acetyl-Coenzyme A concentrations were determined by using a fluorometric kit (MAK039-1KT, Sigma-Aldrich). $CD4^+CD45RO^-$ T cells were stimulated and cultured for 72 h before measurement.

qPCR

RNA extraction and RT-PCR were performed as previously described[39,48]. Primer sequences are listed in Supplementary Table 2. Gene expression was normalized to 18S rRNA.

Immunoblotting

Cellular proteins were extracted using the cOmplete™ Lysis-M EDTA-free from Roche (4719964001, Sigma-Aldrich). Expression levels were examined following standard Western blotting protocols as described[9,39].

Plasmids and transfections

To manipulate *SH3PXD2A* gene expression, 20 nM ON-TARGET plus Human SH3PXD2A siRNA-SMART pool (ID:9644, GE Healthcare Dharmacon Inc), control siRNA (Life Technologies), pECE M2-SH3PXD2A WT (#69813, Addgene), or control vector were transfected into $CD4^+CD45RO^-$ T cells that had previously been stimulated with anti-CD3/CD28 beads for 48 h. For silencing of the *PFKFB3* gene, $CD4^+CD45RO^-$ T cells were stimulated with anti-CD3/CD28 beads for 48 h and then transfected with 20 nM ON-TARGETplus PFKFB3 siRNA-SMART pool (ID:5209, GE Healthcare Dharmacon Inc) or control vector using the Amaxa Nucleofector system and the Human T cell Nucleofector kit (LONZA). Cells were cultured for 24 h under standard conditions before further experiments.

Human synovial tissue-NSG chimeras

NOD.Cg-$Prkdc^{scid}Il2rg^{tm1Wjl}$/SzJ (NSG) mice (Jackson Laboratory, Bar Harbor, ME) were kept in pathogen-free facilities and used at the age of 10–12 wks as previously described[9,36,48]. Briefly, pieces of human synovial tissue free of inflammatory infiltrates were placed into a subcutaneous pocket. After engraftment, mice were reconstituted with 10 million $CD45RO^-$ PBMCs as previously described[9,48]. Mice carrying the same synovial tissue and reconstituted with them same population of $CD45RO^-$ PBMC populations were assigned to parallel treatment arms. The $CD45RO^-$ PBMC derived from (1) RA patients with highly active disease; (2) age-matched healthy controls; (3) $CD45RO^-$ PBMCs from RA patients transfected with *SH3PXD2A* siRNA or control siRNA; (4) $CD45RO^-$ PBMCs from healthy donors transfected with *SH3PXD2A* over-expression plasmids or control vector.

For studies targeting glycolytic flux, chimeric mice were injected with 10 million $CD45^+RO^-$ PBMCs pretreated for 72 h as follows: (A) standard medium (control); (B) PFKFB3 inhibitor 3PO (200 nM); (C) transfected with a *PFKFB3*-specific siRNA. For experiments targeting anabolic lipogenesis, chimeric mice carrying the same synovial tissue were randomly assigned to three treatment arms: (A) control (vehicle); (B) treatment with FAS inhibitor C75 (5 mg/kg/mouse qad, # 191282-48-1 Cayman Chemical); or ML265 (10 mg/kg/mouse qd, #1221186-53-3 Cayman Chemical). Small molecule reagents were delivered by intraperitoneal injection over a period of 7 days.

At completion, synovial tissues were explanted and OCT-embedded (#4583, Sakura Finetek USA) for histology or shock frozen for RNA extraction.

All experiments were carried out in accordance with the guidelines required by the Institutional Animal Care and Use Committee at Stanford University.

Antibodies

Primary antibodies used: APC/Cy7 anti-human CD3 (Clone SK7, BioLegend), FITC anti-human CD4 (Clone RPA-T4, BioLegend), anti-human CD8a PE-Cy5 (Clone RPA-T8, eBioscience), PE-Cy™7 Mouse Anti-Human CD45RA (Clone HI100, BD Biosciences), APC anti-human CD45RA (Clone HI100, BioLegend), APC Mouse Anti-Human CD45RO

(Clone UCHL1, BD Biosciences), Brilliant Violet 711™ anti-human CD45 (HI30, BioLegend), cortactin antibody (PA5-29799) (ThermoFisher Scientific), FAS mouse monoclonal antibody (M01) (Clone 3F2-1F3, Abnova), Acetyl-CoA Carboxylase (C83B10) Rabbit mAb (Cell Signaling Technology), SCD1 (C12H5) Rabbit mAb (Cell Signaling Technology), RANKL/CD254 Antibody (12A668) (ThermoFisher Scientific), Monoclonal Mouse Anti-Human CD3 (Clone F7.2.38, Dako), Polyclonal Rabbit Anti-Human CD3 (#A045201-2, Dako), β-Actin (8H10D10) Mouse mAb (#3700, Cell Signaling), Anti-rabbit IgG, HRP-linked Antibody (#7074, Cell Signaling), WesternSure HRP Goat anti-Mouse IgG (H+L) (LI-COR), Anti-Interferon gamma antibody (ab25101, Abcam), Anti-PPAR gamma antibody (ab178860, Abcam), PPARγ (81B8) Rabbit mAb (Cell Signaling), Monoclonal anti-flag (HRP) antibody (A8592-.2MG, Sigma-Aldrich).

Statistical analysis

All data are presented as mean ± s.e.m. Data were analyzed using GraphPad Prism software. Statistical significance was assessed by paired t-test and Mann-Whitney test, as appropriate. A *P*-value of < 0.05 was considered significant.

Supplementary Material

Refer to Web version on PubMed Central for supplementary material.

Acknowledgments

This work was supported by the National Institutes of Health (R01 AR042527, R01 HL 117913, R01 AI108906 and P01 HL129941 to CMW and R01 AI108891, R01 AG045779, U19 AI057266, and I01 BX001669 to JJG).

References

1. McInnes IB, Buckley CD, Isaacs JD. Cytokines in rheumatoid arthritis - shaping the immunological landscape. Nature reviews. Rheumatology. 2016; 12:63–68. [PubMed: 26656659]
2. Weyand CM, Goronzy JJ. T-cell-targeted therapies in rheumatoid arthritis. Nature clinical practice. Rheumatology. 2006; 2:201–210.
3. McInnes IB, Schett G. The pathogenesis of rheumatoid arthritis. The New England journal of medicine. 2011; 365:2205–2219. [PubMed: 22150039]
4. Weyand CM, Fujii H, Shao L, Goronzy JJ. Rejuvenating the immune system in rheumatoid arthritis. Nature reviews. Rheumatology. 2009; 5:583–588. [PubMed: 19798035]
5. Koetz K, et al. T cell homeostasis in patients with rheumatoid arthritis. Proceedings of the National Academy of Sciences of the United States of America. 2000; 97:9203–9208. [PubMed: 10922071]
6. Schmidt D, Goronzy JJ, Weyand CM. CD4+ CD7- CD28- T cells are expanded in rheumatoid arthritis and are characterized by autoreactivity. The Journal of clinical investigation. 1996; 97:2027–2037. [PubMed: 8621791]
7. Broux B, Markovic-Plese S, Stinissen P, Hellings N. Pathogenic features of CD4+CD28- T cells in immune disorders. Trends Mol Med. 2012; 18:446–453. [PubMed: 22784556]
8. Yang Z, Matteson EL, Goronzy JJ, Weyand CM. T-cell metabolism in autoimmune disease. Arthritis research & therapy. 2015; 17:29. [PubMed: 25890351]
9. Yang Z, et al. Restoring oxidant signaling suppresses proarthritogenic T cell effector functions in rheumatoid arthritis. Science translational medicine. 2016; 8:331ra338.
10. Weyand CM, Yang Z, Goronzy JJ. T-cell aging in rheumatoid arthritis. Current opinion in rheumatology. 2014; 26:93–100. [PubMed: 24296720]

11. Yang Z, Fujii H, Mohan SV, Goronzy JJ, Weyand CM. Phosphofructokinase deficiency impairs ATP generation, autophagy, and redox balance in rheumatoid arthritis T cells. The Journal of experimental medicine. 2013; 210:2119–2134. [PubMed: 24043759]
12. Shao L, et al. Deficiency of the DNA repair enzyme ATM in rheumatoid arthritis. The Journal of experimental medicine. 2009; 206:1435–1449. [PubMed: 19451263]
13. Patra KC, Hay N. The pentose phosphate pathway and cancer. Trends in biochemical sciences. 2014; 39:347–354. [PubMed: 25037503]
14. Wang R, Green DR. Metabolic checkpoints in activated T cells. Nature immunology. 2012; 13:907–915. [PubMed: 22990888]
15. Vander Heiden MG, Cantley LC, Thompson CB. Understanding the Warburg effect: the metabolic requirements of cell proliferation. Science. 2009; 324:1029–1033. [PubMed: 19460998]
16. Menendez JA, Lupu R. Fatty acid synthase and the lipogenic phenotype in cancer pathogenesis. Nature reviews. Cancer. 2007; 7:763–777. [PubMed: 17882277]
17. Pearce EL, Poffenberger MC, Chang CH, Jones RG. Fueling immunity: insights into metabolism and lymphocyte function. Science. 2013; 342:1242454. [PubMed: 24115444]
18. Thiam AR, Farese RV Jr, Walther TC. The biophysics and cell biology of lipid droplets. Nature reviews. Molecular cell biology. 2013; 14:775–786. [PubMed: 24220094]
19. van Meer G, Voelker DR, Feigenson GW. Membrane lipids: where they are and how they behave. Nature reviews. Molecular cell biology. 2008; 9:112–124. [PubMed: 18216768]
20. Marat AL, Haucke V. Phosphatidylinositol 3-phosphates-at the interface between cell signalling and membrane traffic. EMBO J. 2016; 35:561–579. [PubMed: 26888746]
21. Wellen KE, Thompson CB. A two-way street: reciprocal regulation of metabolism and signalling. Nature reviews. Molecular cell biology. 2012; 13:270–276. [PubMed: 22395772]
22. Akram M. Citric acid cycle and role of its intermediates in metabolism. Cell Biochem Biophys. 2014; 68:475–478. [PubMed: 24068518]
23. Robichaud PP, Boulay K, Munganyiki JE, Surette ME. Fatty acid remodeling in cellular glycerophospholipids following the activation of human T cells. Journal of lipid research. 2013; 54:2665–2677. [PubMed: 23894206]
24. O'Sullivan D, et al. Memory CD8(+) T cells use cell-intrinsic lipolysis to support the metabolic programming necessary for development. Immunity. 2014; 41:75–88. [PubMed: 25001241]
25. Zhang X, Nakajima T, Goronzy JJ, Weyand CM. Tissue trafficking patterns of effector memory CD4+ T cells in rheumatoid arthritis. Arthritis and rheumatism. 2005; 52:3839–3849. [PubMed: 16329093]
26. Carman CV, et al. Transcellular diapedesis is initiated by invasive podosomes. Immunity. 2007; 26:784–797. [PubMed: 17570692]
27. Wolf K, Muller R, Borgmann S, Brocker EB, Friedl P. Amoeboid shape change and contact guidance: T-lymphocyte crawling through fibrillar collagen is independent of matrix remodeling by MMPs and other proteases. Blood. 2003; 102:3262–3269. [PubMed: 12855577]
28. Nobes CD, Hall A. Rho GTPases control polarity, protrusion, and adhesion during cell movement. The Journal of cell biology. 1999; 144:1235–1244. [PubMed: 10087266]
29. Uruno T, et al. Activation of Arp2/3 complex-mediated actin polymerization by cortactin. Nature cell biology. 2001; 3:259–266. [PubMed: 11231575]
30. Stylli SS, et al. Nck adaptor proteins link Tks5 to invadopodia actin regulation and ECM degradation. Journal of cell science. 2009; 122:2727–2740. [PubMed: 19596797]
31. Thompson O, et al. Dystroglycan, Tks5 and Src mediated assembly of podosomes in myoblasts. PLoS One. 2008; 3:e3638. [PubMed: 18982058]
32. Krummel MF, Bartumeus F, Gerard A. T cell migration, search strategies and mechanisms. Nature reviews. Immunology. 2016; 16:193–201.
33. Takemura S, Klimiuk PA, Braun A, Goronzy JJ, Weyand CM. T cell activation in rheumatoid synovium is B cell dependent. Journal of immunology. 2001; 167:4710–4718.
34. Murphy DA, Courtneidge SA. The 'ins' and 'outs' of podosomes and invadopodia: characteristics, formation and function. Nature reviews. Molecular cell biology. 2011; 12:413–426. [PubMed: 21697900]

35. Oikawa T, et al. Tks5-dependent formation of circumferential podosomes/invadopodia mediates cell-cell fusion. The Journal of cell biology. 2012; 197:553–568. [PubMed: 22584907]
36. Seyler TM, et al. BLyS and APRIL in rheumatoid arthritis. The Journal of clinical investigation. 2005; 115:3083–3092. [PubMed: 16239971]
37. Kidani Y, et al. Sterol regulatory element-binding proteins are essential for the metabolic programming of effector T cells and adaptive immunity. Nature immunology. 2013; 14:489–499. [PubMed: 23563690]
38. Walsh, MJ., et al. Probe Reports from the NIH Molecular Libraries Program. Bethesda (MD): 2010. ML265: A potent PKM2 activator induces tetramerization and reduces tumor formation and size in a mouse xenograft model.
39. Shirai T, et al. The glycolytic enzyme PKM2 bridges metabolic and inflammatory dysfunction in coronary artery disease. The Journal of experimental medicine. 2016; 213:337–354. [PubMed: 26926996]
40. Marx N. PPARgamma and vascular inflammation: adding another piece to the puzzle. Circ Res. 2002; 91:373–374. [PubMed: 12215484]
41. Pearce EL, et al. Enhancing CD8 T-cell memory by modulating fatty acid metabolism. Nature. 2009; 460:103–107. [PubMed: 19494812]
42. Nobile C, et al. HIV-1 Nef inhibits ruffles, induces filopodia, and modulates migration of infected lymphocytes. Journal of virology. 2010; 84:2282–2293. [PubMed: 20015995]
43. Hwang SH, et al. Leukocyte-specific protein 1 regulates T-cell migration in rheumatoid arthritis. Proceedings of the National Academy of Sciences of the United States of America. 2015; 112:E6535–6543. [PubMed: 26554018]
44. Buck MD, O'Sullivan D, Pearce EL. T cell metabolism drives immunity. The Journal of experimental medicine. 2015; 212:1345–1360. [PubMed: 26261266]
45. Zeng H, et al. mTORC1 couples immune signals and metabolic programming to establish T(reg)-cell function. Nature. 2013; 499:485–490. [PubMed: 23812589]
46. Takemura S, et al. Lymphoid neogenesis in rheumatoid synovitis. Journal of immunology. 2001; 167:1072–1080.
47. Nakano A, et al. AMPK controls the speed of microtubule polymerization and directional cell migration through CLIP-170 phosphorylation. Nature cell biology. 2010; 12:583–590. [PubMed: 20495555]
48. Li Y, et al. Deficient Activity of the Nuclease MRE11A Induces T Cell Aging and Promotes Arthritogenic Effector Functions in Patients with Rheumatoid Arthritis. Immunity. 2016; 45:903–916. [PubMed: 27742546]

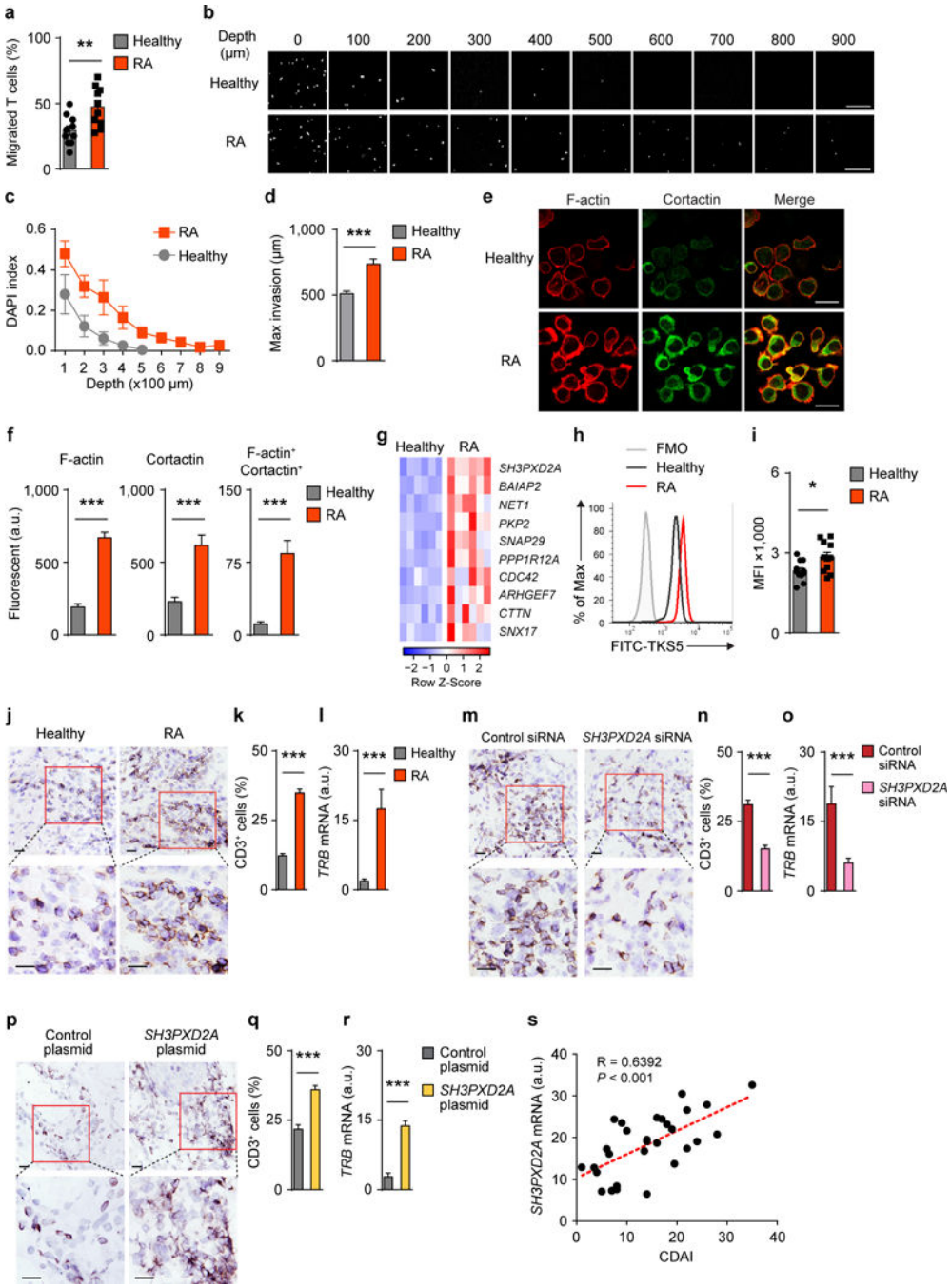

Figure 1. Hypermotility and tissue-invasiveness of RA T cells

(**a**) Migration of activated $CD4^+CD45RA^+$ T cells in transwells without chemokines for 48 h (n=10). (**b–d**) $CD4^+$ T cells invasiveness in 3D-collagen matrices measured by confocal imaging DAPI-stained nuclei. (**b**) Representative confocal images at indicated depths after 48 h. Scale bar, 200 μm. (**c**) DAPI indices (signal at defined depth/signal at surface) (5 control-RA pairs). (**d**) Maximum invasion distances (n=5). (**e, f**) Cytoskeletal organization and membrane protrusions analyzed by confocal microscopy. Membrane ruffles and podosomes identified through F-actin/cortactin co-localization. (**e**) Representative

micrographs showing actin mesh co-localizing with cortactin in lamellopodia and membrane ruffles. Scale bars, 20 μm. (**f**) Quantification of F-actin, cortactin and F-actin^{+}cortactin^{+} membrane protrusions (5 control-RA pairs). (**g**) Gene expression profiling (RT-PCR) of genes involved in actin nucleation and cell motility. Heat map presentation from 6 RA-control pairs. Scaled z-score: red indicates high and blue low transcript levels. (**h–i**) Representative histograms and bar graphs of T cell TKS5 protein expression (11 control-RA pairs). (**j–l**) Human synovium-NSG mice (n=14) were reconstituted with CD4^{+}CD45RO^{-} PBMC from healthy individuals or RA patients. (**j**) Immunohistochemistry of synovial CD3^{+} T cells, scale bars, 20 μm. (**k**) Tissue-invading T cells as percentage of total cells. (**l**) T cell receptor (*TRB*) transcript concentrations. (**m–o**) Human synovium-NSG chimeras (n=14) were reconstituted with RA CD4^{+}CD45RO^{-} PBMC transfected with *SH3PXD2A* or control siRNA. (**m**) Immunohistochemistry of synovial CD3^{+} T cells. (**n**) Number of tissue-invading T cells. (**o**) *TRB* transcript concentrations. (**p–r**) Human synovium-NSG chimeras (n=14) were reconstituted with healthy CD4^{+}CD45RO^{-} PBMC transfected with *SH3PXD2A* or control plasmids. (**p, q**) Immunohistochemistry of synovial CD3^{+} T cells. (**r**) T cell receptor (*TRB*) transcript concentrations. (**s**) RA disease activity assessed by the Clinical Disease Activity Index (CDAI) correlated with TKS5 transcripts in activated CD4^{+}CD45RA^{+} T cells. Data from 29 patients. All data are mean ± s.e.m. *P<0.05, **P<0.01, ***P<0.001 (Mann-Whitney U-test).

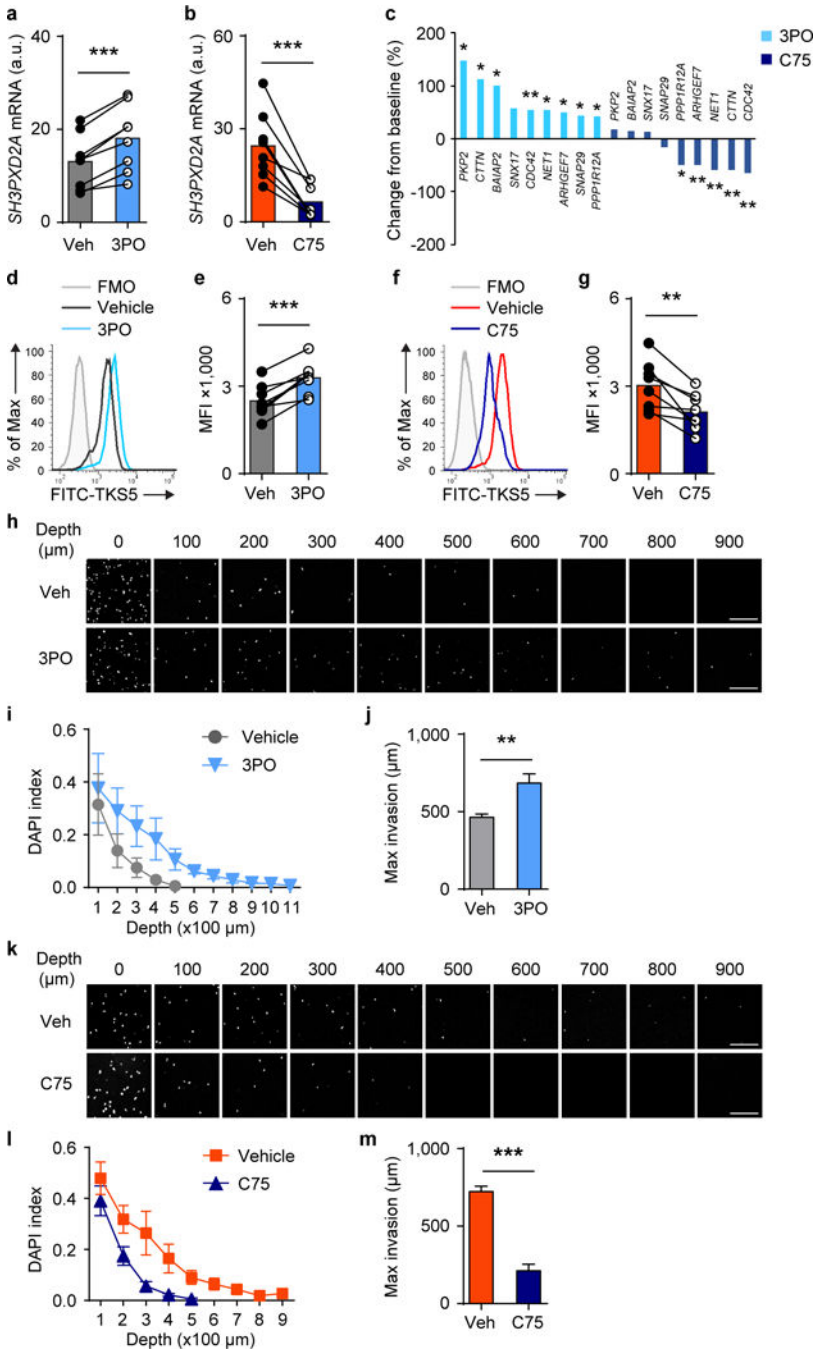

Figure 2. TKS5 expression is metabolically regulated

$CD4^+CD45RA^+$ T cells from healthy individuals were stimulated in the absence or presence of 3PO (200 nM), an inhibitor of the glycolytic enzyme PFKFB3, or C75 (20 μM), an inhibitor of the fatty acid synthase (FAS). (**a, b**) Expression of the *SH3PXD2A* gene assessed by RT-PCR (8 control-RA pairs). (**c**) Expression of the mobility gene module (see Fig. 1) assessed by RT-PCR. Percent change from the vehicle control is shown for each individual gene (8 RA-control pairs). (**d–g**) TKS5 protein expression determined by flow cytometry. Representative histograms and summary from 8 experiments. In **a–c**, **e** and **g**,

data are mean ± s.e.m. * $P < 0.05$, ** $P < 0.01$, *** $P < 0.001$ (paired *t*-test). (**h–m**) T cell invasion measured in the 3D-collagen matrix system as in Fig. 1. (**h**, **k**) Representative confocal images of DAPI-stained nuclei taken at indicated depths. Scale bars, 200 μm. (**i, l**) DAPI indices (signal at defined depth/signal at surface) quantified in 4 experiments. (**j, m**) Maximum invasion distances determined in 4 healthy and 4 RA samples. In **j** and **m**, data are mean ± s.e.m. ** $P < 0.01$, *** $P < 0.001$ (Mann-Whitney U-test).

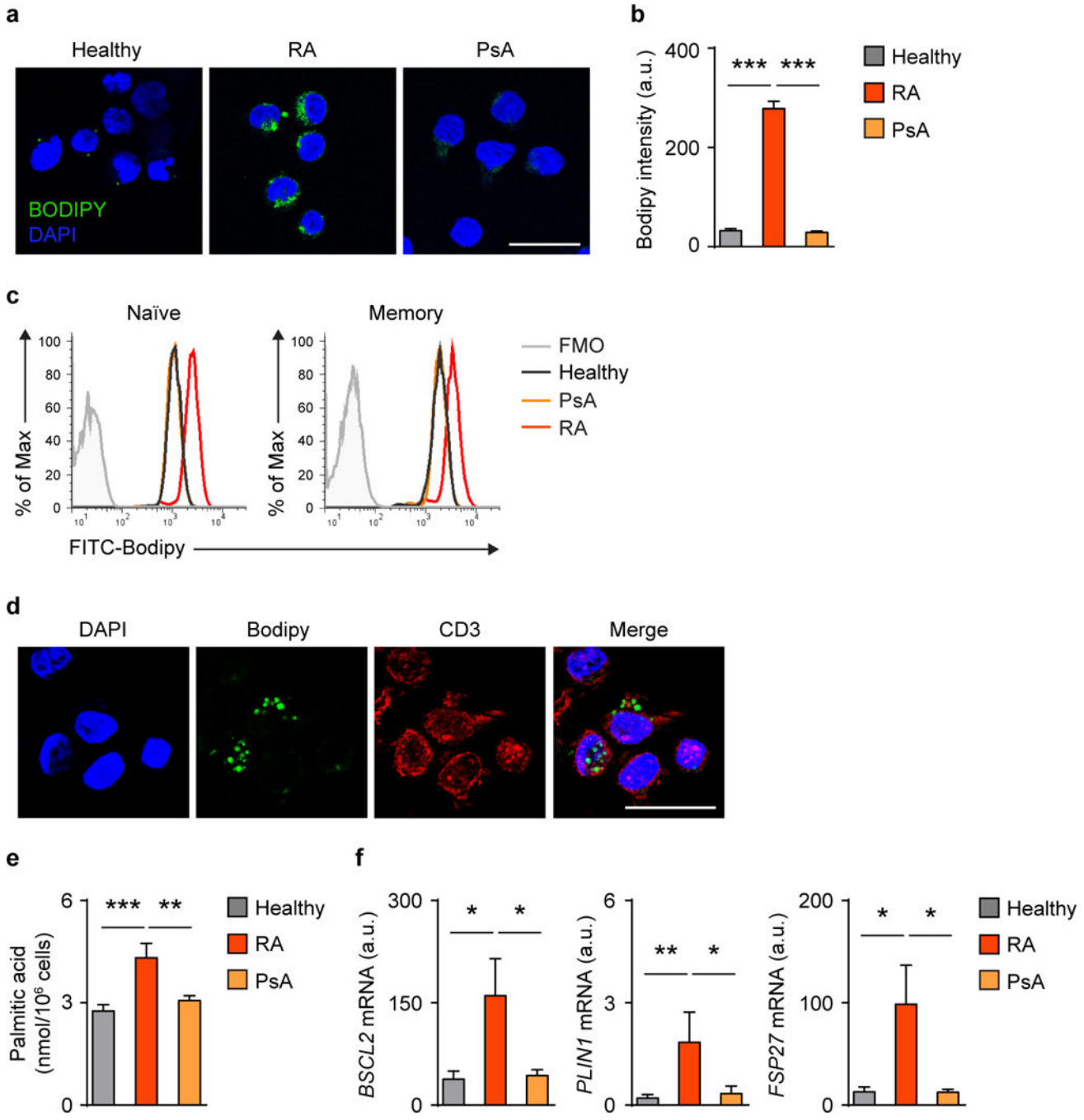

Figure 3. CD4 T cells from RA patients accumulate cytoplasmic lipid droplets

$CD4^+CD45RA^+$ T cells from RA patients and age-matched healthy individuals were stimulated for 96 h and stained with BODIPY (493/503) to quantify intracellular lipids. (**a**) Confocal microscopy imaging of intracellular lipid droplets (green) in RA $CD4^+$ T cells. Scale bar, 20 μm. (**b**) Fluorescent Bodipy quantification in activated $CD4^+CD45RA^+$ T cells from 10 RA patients, 6 PsA patients and 10 healthy individuals. (**c**) Intracellular neutral lipids labeled with Bodipy in naive and memory populations of $CD4^+$ T cells from healthy controls, RA patients and PsA patients. Representative histograms from 3 experiments. (**d**)

Frozen sections from RA synovial tissues were stained with Bodipy (493/503) and analyzed by fluorescence microscopy. Representative images show accumulation of lipid droplets (green) in tissue-residing $CD3^+$ T cells (red). Scale bar, 20 μm. (**e**) Palmitic acid measured in activated $CD4^+CD45RA^+$ T cells from 8 RA patients, 8 healthy donors and 4 PsA patients. (**f**) Expression levels of genes involved in lipid droplet formation from 6 RA patients, 5 PsA patients and 6 controls. All data are mean ± s.e.m. $*P<0.05$, $**P<0.01$, $***P<0.001$ (Mann-Whitney U-test).

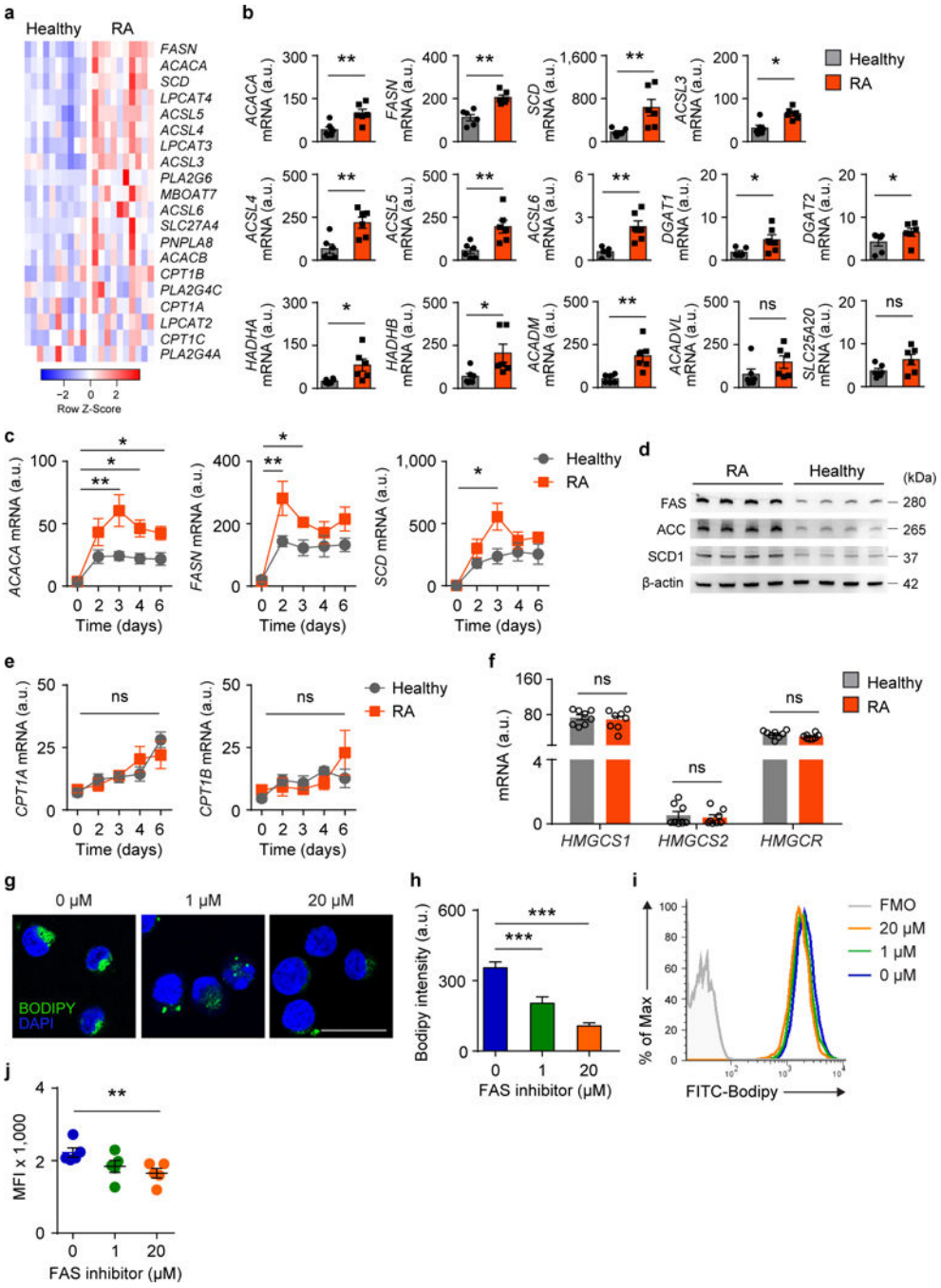

Figure 4. RA CD4$^+$ T cells favor the anabolic lipogenesis program

CD4$^+$CD45RA$^+$ T cells from healthy age-matched individuals and RA patients were stimulated for 72 h. (**a**) Gene expression for 20 lipogenic genes was profiled by RT-PCR. Data from a discovery cohort of 10 healthy-RA pairs are shown as a heat map. Scaled z-score: red indicates high and blue low transcript levels. (**b**) Gene sets of de novo fatty acid synthesis, esterification, and FA β-oxidation pathways compared in a validation cohort of 6 healthy-RA pairs. Relative gene expression measured by RT-PCR. (**c**) Expression kinetics of lipid biosynthesis genes following T cell activation (n = 6 independent samples per time

point). (**d**) Immunoblot analysis of key enzymes involved in FA synthesis (ACC, FAS, SCD1) in 4 control-RA pairs. Data are representative for 8 experiments. (**e**) Expression kinetics of carnitine acyltransferases (*CPT1A* and *CPT1B*, involved in lipid transport into mitochondria) following T cell activation ($n = 5$ independent samples per time point). (**f**) Expression levels of genes involved in cholesterol synthesis (8 healthy-RA pairs). (**g, h**) Representative images showing lipid droplets deposited in the cytoplasm. Fluorescent signal quantification of neutral lipids in C75 treatment groups ($n = 5$ patients/group). Scale bar, 20 μm. (**i, j**) Flow cytometry of Bodipy-stained T cells. Left: Representative histograms. Right: Mean fluorescence intensities from 5 experiments. All data are mean ± s.e.m. $*P < 0.05$. $**P < 0.01$ (Mann-Whitney U-test). Non-significant (ns). FA, fatty acid; MUFA, mono-unsaturated fatty acid; DG, diacylglycerol; TG, triacylglycerol.

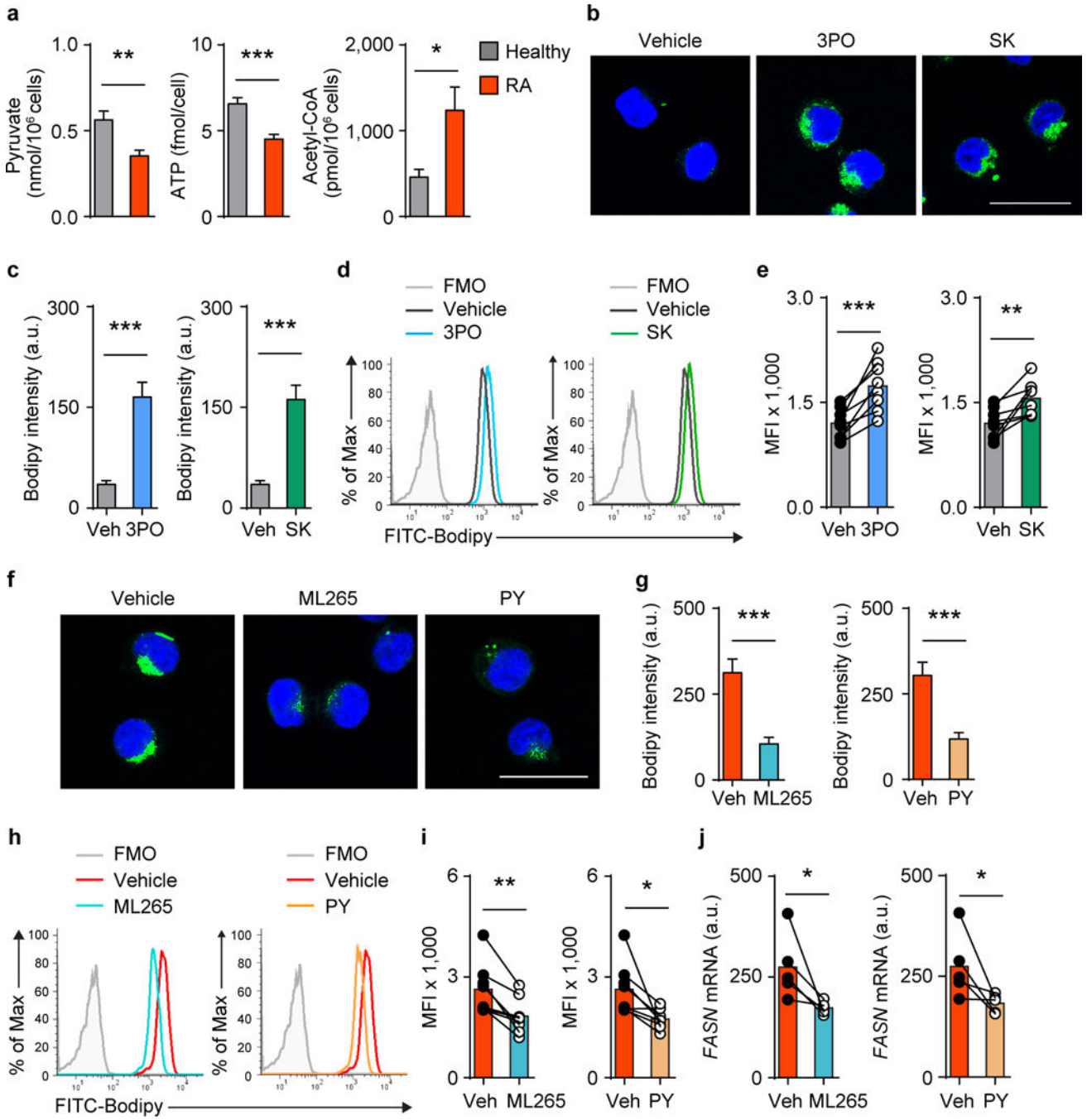

Figure 5. Lipid droplet accumulation is regulated by glycolytic flux and pyruvate availability

$CD4^+CD45RA^+$ T cells from RA patients and age-matched controls were isolated and stimulated for 72 h. (**a**) Pyruvate, intracellular ATP and acetyl-CoA were measured in T cell extracts (9 patient-control pairs for Pyruvate measurements; 17 patient-control pairs for ATP measurements; 6 patient-control pairs for acetyl-CoA measurements). Data are mean ± s.e.m. $*P < 0.05$, $**P < 0.01$, $***P < 0.001$ (Mann-Whitney U-test). (**b–e**) Glycolytic flux was suppressed in healthy $CD4^+CD45RA^+$ T cells by treating with the PFKFB3 inhibitor 3PO (200 nM) or the PKM2 inhibitor Shikonin (SK, 250 nM). (**f–i**) Glycolytic flux was

enhanced in RA $CD4^+CD45RA^+$ T cells by activating PKM2 with ML265 (10 μM) and glycolysis-related energy production was augmented by supplementing pyruvate (PY, 1 μM). Intracellular lipid stores were quantified in Bodipy-stained cells by confocal microscopy. Representative images in **b** and **f**, summary results from 6 experiments in **c** and **g**. Scale bars, 20 μm. Alternatively, Bodipy staining was quantified by flow cytometry. Representative histograms in **d** and **h**, summary results from 8 experiments in **e** and **i**. Data are mean ± s.e.m. $*P < 0.05$, $**P < 0.01$, $***P < 0.001$ (Mann-Whitney U-test (**c**, **g**) or paired *t*-test (**e**, **i**)). (**j**) FASN transcripts were measured by RT-PCR in $CD4^+CD45RA^+$ T cells treated with vehicle, ML265 or pyruvate (PY) in 5 independent experiments. Data are mean ± s.e.m.$*P < 0.05$ (Mann-Whitney U-test).

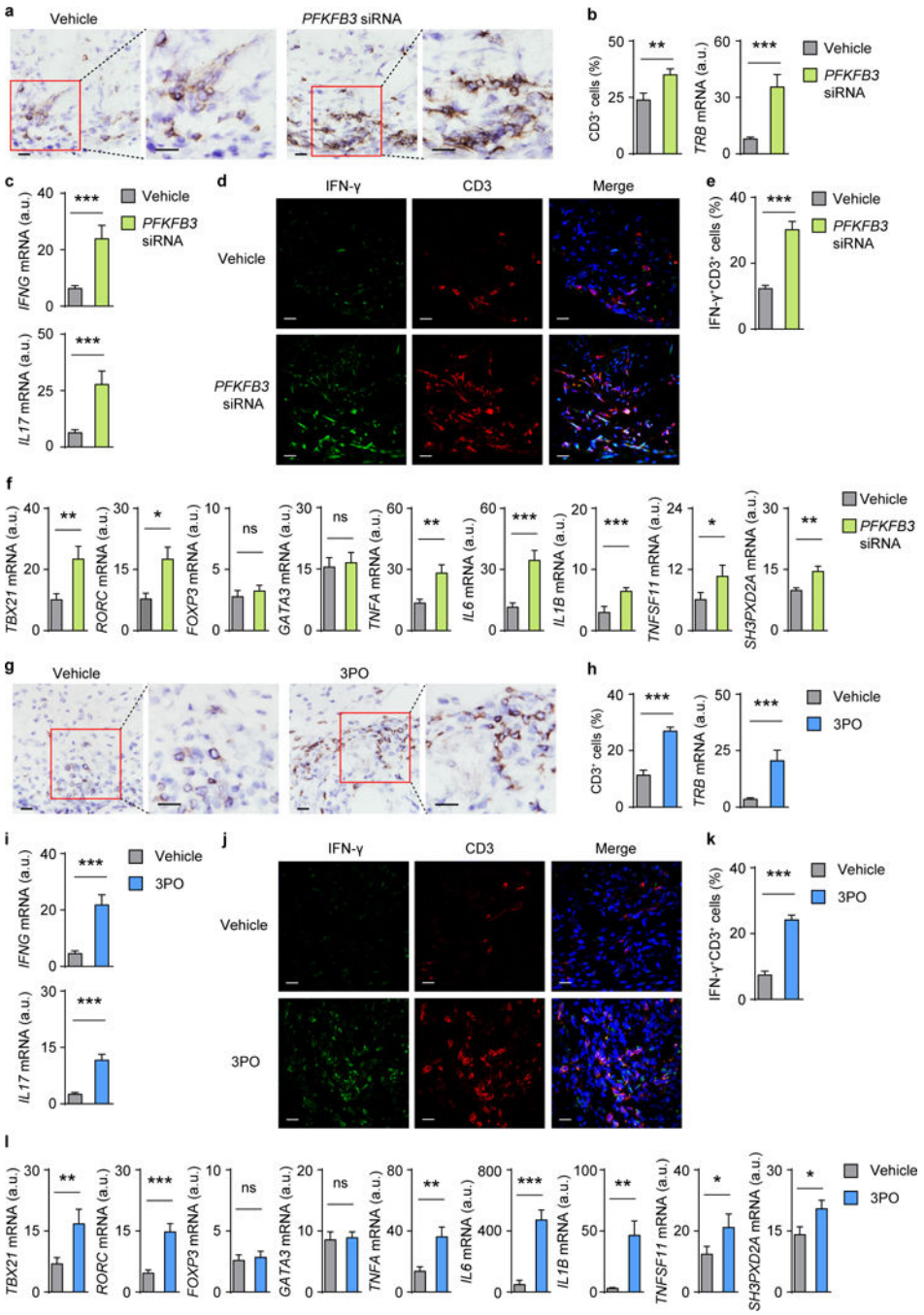

Figure 6. Reducing glycolytic flux renders CD4$^+$ T cells tissue-invasive and pro-inflammatory

CD4$^+$CD45RO$^-$ PBMC were isolated from healthy individuals. Glycolytic activity was inhibited by transfecting the cells with PFKFB3 siRNA (**a–f**) or treating with the PFKFB3 inhibitor 3PO (200 nM) (**g–l**). Cells were adoptively transferred into human synovium-engrafted NSG mice. Seven days later, synovial tissue grafts were harvested and processed for immuno-histochemical analysis or for RT-PCR analysis of cytokine and transcription factor gene expression. Data indicate mean ± s.e.m. from 20 different synovial tissues. (**a**, **g**) Immunohistochemical staining for tissue-residing CD3$^+$ T cells. Scale bars, 20 μm. (**b**, **h**)

Quantification of T cell receptor (*TRB*) transcripts and of tissue-invading $CD3^+$ T cells, expressed as percent of total cells. (**c**, **i**) Gene expression of *IFNG* and *IL17*. (**d**, **j**) Co-immunofluorescence staining of tissue sections for IFN-γ and $CD3^+$ T cells. Scale bars, 20 μm. (**e**, **k**) Frequencies of IFN-γ^+ $CD3^+$ T cells in the tissue. (**f**, **l**) Gene expression of lineage-determining transcription factors, key inflammatory markers and TKS5 were determined by RT-PCR. Scale bars, 20 μm. All data are mean ± s.e.m. $*P < 0.05$. $**P < 0.01$. $***P < 0.001$(Mann-Whitney U-test). Non-significant (ns).

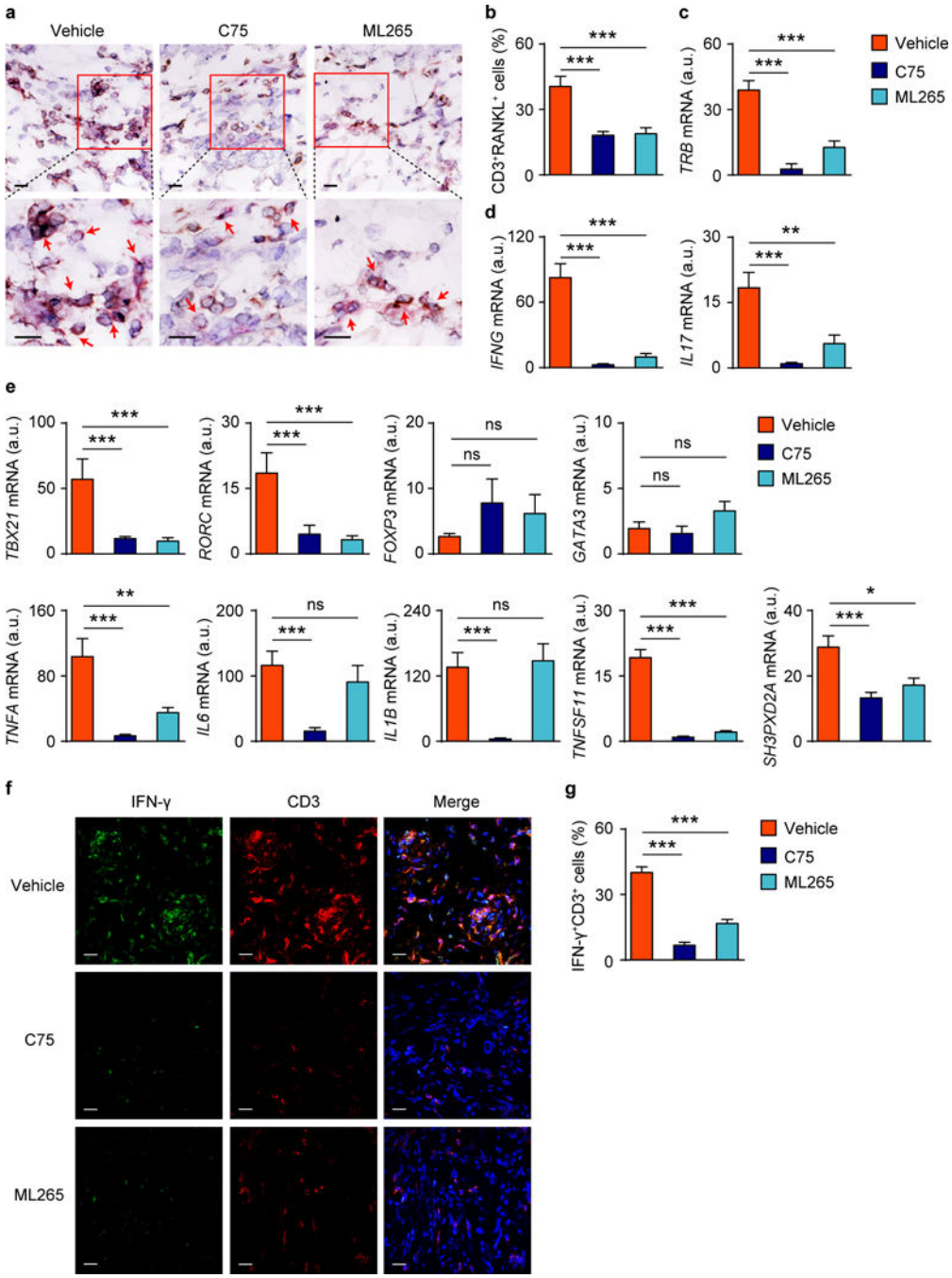

Figure 7. Inhibiting fatty acid synthesis or accelerating pyruvate generation corrects the tissue-invasive and arthritogenic behavior of RA T cells

$CD4^+CD45RO^-$ PBMC were isolated from RA patients with active disease and adoptively transferred into human synovium-NSG chimeric mice. Mice were randomly assigned to one of three treatment arms ($n = 14$ synovial grafts/treatment arm): Vehicle arm (vehicle injection); RA treated with C75 (5 mg/kg, i.p. every other day) or RA treated with ML265 (10 mg/kg, i.p. daily). Synovial tissues were harvested, tissue sections were stained with anti-human CD3 (brown) and anti-RANKL (pink) antibodies and frequencies of RANKL

positive cells were quantified in randomly selected high-powered fields. (**a**) Representative tissue stains showing human $CD3^+$ and $RANKL^+$ T cells infiltrating into synovial tissue, where they form cellular clusters. Scale bars, 20 μm. (**b**) Frequencies of $CD3^+RANKL^+$ T cells in the tissue as percent of total cells. (**c**) RT-PCR-based quantification of T cell receptor (*TRB*) transcripts. (**d**) Gene expression of *IFNG* and *IL17*. (**e**) Gene expression of transcription factors, key cytokines and TKS5 determined by RT-PCR. (**f**, **g**) Co-immunofluorescence staining of tissue sections for IFN-γ and CD3. Frequencies of tissue-residing IFN-γ^+ $CD3^+$ T cells in the different treatment arms. Scale bars, 20 μm. All data are mean ± s.e.m. * $P < 0.05$. ** $P < 0.01$. *** $P < 0.001$ (Mann-Whitney U-test). Non-significant (ns).